




Ferromagnetic impurity induced Majorana zero mode in iron-based superconductorsRui Song ^{1,2,3}, Ping Zhang,^{4,2,5,*} Xian-Tu He,^{2,5} and Ning Hao ^{3,†}¹*HEDPS, Center for Applied Physics and Technology and School of Physics, Peking University, Beijing 100871, China*²*HEDPS, Center for Applied Physics and Technology and School of Engineering, Peking University, Beijing 100871, China*³*Anhui Key Laboratory of Condensed Matter Physics at Extreme Conditions, High Magnetic Field Laboratory, HFIPS, Anhui, Chinese Academy of Sciences, and University of Science and Technology of China, Hefei 230031, China*⁴*School of Physics and Physical Engineering, Qufu Normal University, Qufu 273165, China*⁵*Institute of Applied Physics and Computational Mathematics, Beijing 100088, China* (Received 11 April 2022; revised 9 October 2022; accepted 2 November 2022; published 10 November 2022)

Recent experiments reported the puzzling zero-energy modes associated with ferromagnetic impurities in some iron-based superconductors with topological band structures. Here, we show that a sufficiently strong exchange coupling between a ferromagnetic impurity and a substrate can trigger a quantum phase transition, beyond which the phase of the topological surface superconducting order parameter around the impurity acquires a sign change. In such a case, we prove that besides a pair of impurity induced trivial Yu-Shiba-Rusinov states, a degenerate pair of Majorana modes can be induced at the boundary separating the two sign-change regimes and trapped around the impurity in the topological surface superconducting state. Furthermore, we show that our theory can explain the controversial observations and confusing features of the zero-energy modes from recent experiments in some iron-based superconductors.

DOI: [10.1103/PhysRevB.106.L180504](https://doi.org/10.1103/PhysRevB.106.L180504)

In superconductors, impurities can induce various quasi-particle states, such as the Yu-Shiba-Rusinov (YSR) state from the classical impurity scattering potential [1–3] and the Kondo resonance state from impurities in the quantum limit [4]. Through elucidating their properties, one can obtain much critical information on electron pairing [5]. Meanwhile, the quasiparticle state itself can manifest some unexpected behaviors. In particular, an interstitial iron impurity (IFI) induced robust zero-energy mode (ZM) has been reported by scanning tunneling microscopy and spectroscopy (STM and STS) in the iron-based superconductor Fe(Te,Se) [6]. Subsequent studies have been extended to other iron-based superconductors such as monolayer Fe(Te,Se)/SrTiO₃ and LiFeAs, and a similar ZM is observed there also [7,8]. Experimentally, the ZM can only be observed on partial iron impurities and is robust against the external magnetic field, and the critical temperature is much below the superconducting transition temperature T_c . Besides, these materials share a remarkable feature of possessing topological bands, which implies that the ZMs could be Majorana modes. In contrast, some revisited studies on Fe(Te,Se) claim that the observed ZMs are just trivial YSR states with near-zero-energy electronlike and holelike components [9,10]. Thus the properties and the mechanism of the ZMs in these iron-based superconductors are still under debate [6–10].

In this Research Letter, we first perform first-principles calculations to investigate the interaction between an IFI and the substrate FeSe_{0.45}Te_{0.55}. The numerical results indicate that the exchange coupling $J(\mathbf{r}, z)$ between the magnetic moment

of the IFI and the spin of the 3d electrons of FeSe_{0.45}Te_{0.55} has the form of Friedel-like oscillations with characteristic length a_0 of the lattice constant of the iron square lattice. The amplitude of $J(\mathbf{r}, z)$ and the magnetic moment of the IFI strongly depend on the height z between the IFI and the substrate. We further consider the impact of the IFI on the topological surface superconducting order parameter $\Delta(\mathbf{r})$ by solving the Bogoliubov–de Gennes (BdG) equations describing the topological surface superconductivity and defined on the iron square lattice with self-consistency. We find that there exists a quantum phase transition (QPT) at a critical height z_c , i.e., a critical $J_c(\mathbf{r}, z_c)$, beyond which $\Delta(\mathbf{r})$ changes sign in the $r < a_0$ regime. Then, we prove that besides a pair of impurity induced trivial YSR states, a Kramers degenerate pair of Majorana ZMs can be induced at the boundary separating the two sign-change regimes and trapped by the IFI. For the smaller $J(\mathbf{r}, z) < J_c(\mathbf{r}, z_c)$, the QPT cannot be triggered. The IFI can only induce trivial YSR states, which have near-zero energy in the vicinity of the QPT. Within this picture, the contradictions between the results from different STM and STS measurements can be resolved, and properties of the ZMs, such as robustness against the external magnetic field and lower critical temperature, can also be understood.

STM experiments show that the height of an IFI can be tuned by the STM tip [8,10]. During the process of approaching, the transition from YSR states to ZMs happens [8]. This indicates that the coupling between the IFI and the substrate plays a crucial role in observing ZMs. To elucidate the properties of such coupling, we construct a $9 \times 9 \times 1$ supercell including the substrate Fe(Te,Se) with a suspended IFI. In Fig. 1, we only summarize the main results, and calculation details are given in the Supplemental Material [11]. From Fig. 1(a), we see that there exists a strong charge transfer between the IFI and the substrate iron atoms, and such transfer

*zhang_ping@iapcm.ac.cn

†haon@hmfl.ac.cn

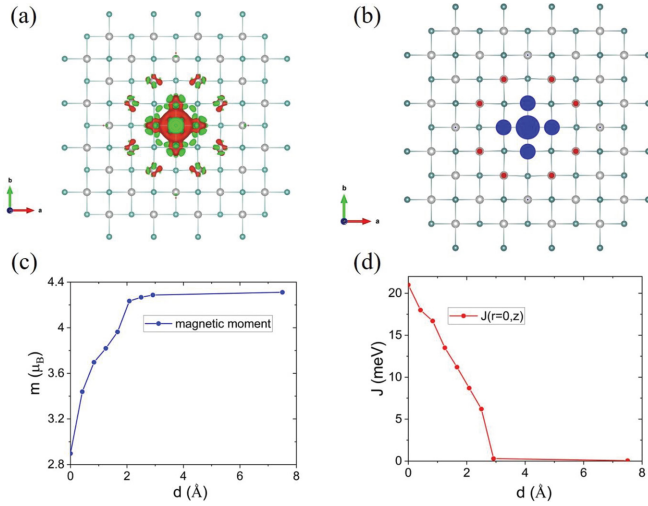


FIG. 1. (a) The spatial distributions of the differential charge density of a supercell involving a $9 \times 9 \times 1$ Fe(Te,Se) substrate and a suspended IFI. (b) The spatial distributions of the induced spin polarizations of the $3d$ electrons of iron atoms in the substrate. The size and color of the dots denote the strength and direction of the spin polarization, respectively. (c) and (d) The magnetic moment of the IFI and the effective exchange coupling $J(r=0, z)$ as a function of the height d between the IFI and the substrate, respectively.

decays abruptly as expected. The calculated spin polarizations of the substrate shown in Fig. 1(b) indicate that $J(\mathbf{r}, z_0)$ has the form of Friedel-like oscillations, which is consistent with a neutron scattering experiment on Fe(Te,Se) with a higher concentration of Te [24]. The characteristic length of the measured oscillation period is about equal to the lattice constant a_0 as seen from Fig. 1(b). These findings are further supported by the magnetic moment of the IFI as a function of height, as shown in Fig. 1(c). As the IFI approaches the substrate, the magnetic moment of the IFI is suppressed. This indicates that spin transfer also happens and that the exchange coupling between the magnetic moment of the IFI and the substrate is strong. The strength of $J(\mathbf{r} = 0, z_0)$ can be roughly estimated and is shown in Fig. 1(d) [11].

Another crucial experimental signature is the presence of a level crossing at the transition from YSR states to ZMs, and the level crossing is robust against the magnetic field [8]. This signature indicates that a suitable model related to STS experiments is that of topological surface Dirac bands with trivial s -wave pairing, and the model of trivial bulk bands with S_{\pm} pairing fails (see Supplemental Material [11]). Thus we start with such a model defined on square lattices to evaluate impact of the IFI on the $\Delta(\mathbf{r})$ of topological Dirac states on the surface of the Fe(Te,Se) substrate. The model Hamiltonian is

$$H_{\text{eff}} = H_{\text{BdG}} + H_{\text{coup}}, \quad (1)$$

where

$$H_{\text{BdG}} = -\mu \sum_i c_i^\dagger c_i - it \sum_{(i,j)} c_{i\sigma}^\dagger (\mathbf{S}^{\sigma\sigma'} \times \hat{\mathbf{d}}_{ij}) \cdot \hat{\mathbf{z}} c_{j\sigma'} + \sum_i \Delta_i (c_{i\uparrow}^\dagger c_{i\downarrow}^\dagger + \text{c.c.}), \quad (2)$$

$$H_{\text{coup}} = \int d\mathbf{r} J(\mathbf{r}, z_0) \mathbf{S}_{\text{imp}} \cdot \boldsymbol{\sigma}. \quad (3)$$

Here, μ is the chemical potential. The second term in Eq. (2) describes the topological surface Dirac states defined on square lattices. $\hat{\mathbf{d}}_{ij}$ is the unit vector pointing from i to j . Δ_i is the site-dependent superconducting order parameter. Note that such trivial s -wave pairing is a good approximation for the topological surface Dirac state, can give results that are consistent with STS experiments [8,11], and is widely adopted to study the topological properties of iron-based superconductors [23,25–32]. This indicates that STM and STS only detect the surface physics and have a distant relationship with possible bulk S_{\pm} pairing. \mathbf{S}_{imp} and $\boldsymbol{\sigma}$ in Eq. (3) label the magnetic moment of the IFI and the spin of the Fe of the substrate, respectively. Here, we only consider z -directional spin polarization. $J(\mathbf{r}, z_0)$ is important only in the first oscillating period a_0 . The nearest-neighbor $J(\mathbf{r}, z_0)$ is less than J_c according to the calculation. Here, we only consider the on-site term $J(\mathbf{r} = 0, z_0)$ for simplicity [11]. As $J(\mathbf{r} = 0, z_0)$ increases from zero, there exists a QPT [5,33,34] at a critical $J_c \sim 1.3t$, beyond which $\Delta(r)$ suddenly changes sign and becomes negative, as shown in Fig. 2(b). Meanwhile, the level crossing of two components of YSR states happens, as shown in Fig. 2(a). Then, the spatial distributions of $\Delta(r)$ in Fig. 2(c) indicate that $\Delta(r)$ acquires a π phase difference in the $r < R_0$ regime in comparison to that in the $r > R_0$ regime. Note that R_0 can take the value of lattice constant a_0 if the nearest-neighbor term of $J(\mathbf{r}, z_0)$ is involved [11]. This is a very crucial result regarding the effect of IFIs [33–37]. Though the QPT is not driven by temperature, an increase in temperature could quench it. Therefore we calculate the critical temperature T_q of the QPT and find that T_q is quite lower than the bulk superconducting transition temperature T_c . We will return to this temperature effect below.

Now, we consider the effect of spatial variation of $\Delta(r)$ of the topological surface superconductivity. The effective

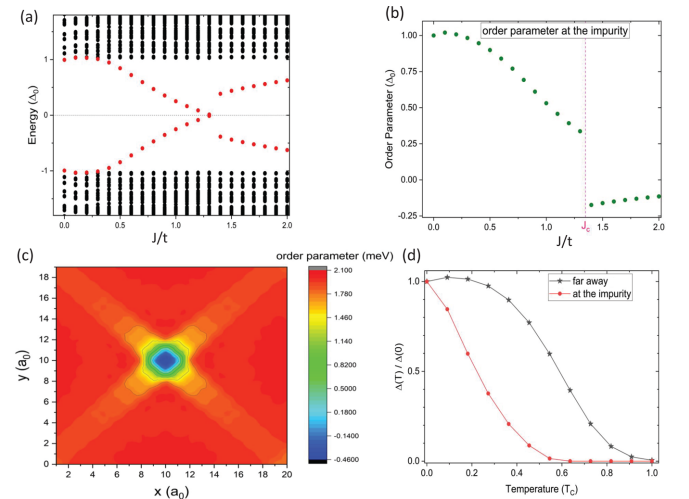


FIG. 2. (a) The energy spectrum as a function of $J(r=0, z)$ from the self-consistent solution of Eq. (1). The red dots with opposite energy are a pair of YSR states. (b) The order parameter of the superconducting state $\Delta(r=0)$ as a function of $J(r=0, z)$ from the self-consistent solution of Eq. (1). (c) The spatial distributions of $\Delta(r)$ under the condition $J(r=0, z) = 1.5t$. (d) The temperature evolution of $\Delta(r)$ from the self-consistent solution of Eq. (1).

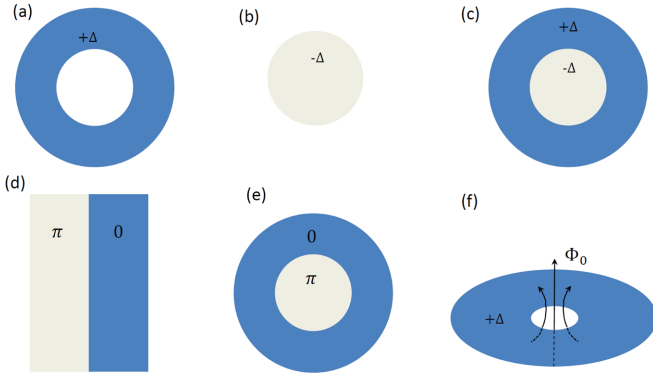


FIG. 3. (a) The infinite ring with uniform positive superconducting pairing Δ . (b) The finite disk with uniform negative superconducting pairing $-\Delta$. (c) Our $0-\pi$ disk junction is the spatial combination of (a) and (b). (d) and (e) The $0-\pi$ line junction bends to form a $0-\pi$ disk junction that is the same as the one in (c). (f) The infinite disk with uniform positive superconducting pairing Δ , which has a centric hole with superconducting flux quanta.

Hamiltonian describing the topological surface superconductivity with the sign-change boundary condition is

$$H_s = [v_F(\mathbf{k} \times \boldsymbol{\sigma}) \cdot \hat{\mathbf{z}} - \mu]\tau_z + \Delta(r)\tau_x. \quad (4)$$

Here, H_s is spanned in the Nambu space, i.e., $[c_\uparrow, c_\downarrow, c_\downarrow^\dagger, -c_\uparrow^\dagger]$. $\tau_{x/z}$ is the Pauli matrix to span the particle-hole space. $\Delta(r) = -\Delta_1$ when $r < R_0$, and $\Delta(r) = \Delta_2$ when $r > R_0$ with $\Delta_{1/2} > 0$ and $\Delta_1 < \Delta_2$. The phase of $\Delta_{1/2}$ is uniform and is omitted due to the absence of topological defects such as a vortex. Thus $\Delta_{1/2}$ is angle independent, and $\Delta(r)$ is real in Eq. (4). In the continuum limit, the eigenequation of H_s is

$$H_s(\mathbf{k} \rightarrow -i\nabla)\psi(r, \theta) = E\psi(r, \theta), \quad (5)$$

which can be solved under boundary conditions with a $0-\pi$ disk junction as shown in Fig. 3(c).

Before solving Eq. (5), we give a simple physical picture to understand the existence of a Kramers degenerate pair of Majorana ZMs of the model. The Hamiltonian in Eq. (4) preserves particle-hole symmetry (PHS) with $\mathcal{C} = i\sigma_y\tau_yK$ and time-reversal symmetry (TRS) with $\mathcal{T} = i\sigma_y\tau_0K$. The $0-\pi$ disk junction in Fig. 3(c) can come from the combination of the geometries in Figs. 3(a) and 3(b). We know that the geometries in Figs. 3(a) and 3(b) do not host any edge bound states due to the Dirac cone itself being a two-dimensional boundary state [11]. However, when the two geometries in Figs. 3(a) and 3(b) are combined to form the $0-\pi$ disk junction in Fig. 3(c), edge bound states must emerge. This behavior can be understood from Figs. 3(d) and 3(e). The $0-\pi$ disk junction in Fig. 3(e) can also be obtained by bending the $0-\pi$ line junction in Fig. 3(d) to connect the two ends. It is well known that the $0-\pi$ line junction can support the one-dimensional linear-dispersion bound states [38,39]. Likewise, the $0-\pi$ disk junction in Figs. 3(c) and 3(e) should also have edge bound states. Such a difference between Figs. 3(a) and 3(b) and Figs. 3(c) and 3(e) lies in that the wave function $\psi(r, \theta)$ in the $0-\pi$ disk junction in Figs. 3(c) and 3(e) must obey the crucial *antiperiodic boundary condition*, i.e., $\psi(r, \theta) = -\psi(r, \theta + 2\pi)$

to get bound states, which is explicitly pointed out by Fu and Kane [38]. Further considering geometry changes from Fig. 3(d) and 3(e), the one-dimensional linear-dispersion bound states have to split into a series of quantized modes labeled by quantum numbers of angular momentum, among which a pair of Majorana ZMs must emerge. Such emergence can be understood from the vortex case shown in Fig. 3(f). The single-value condition requires that the wave function in the vortex case is *periodic*, i.e., $\psi_v(r, \theta) = \psi_v(r, \theta + 2\pi)$. If one does a gauge transformation $\psi_v(r, \theta) \rightarrow e^{i\sigma_z\theta/2}\psi'_v(r, \theta)$, the phase winding of the superconducting pair is eliminated, and the new wave function $\psi'_v(r, \theta)$ must obey the *antiperiodic boundary condition* $\psi'_v(r, \theta) = -\psi'_v(r, \theta + 2\pi)$ [11]. This means that applying magnetic flux is equivalent to changing the boundary conditions of the wave function [40]. In this sense, our case is made equivalent to the vortex case by further taking into account another time-reversal counterpart [11]. Therefore Majorana ZMs must emerge for the Hamiltonian in Eq. (4) with the $0-\pi$ disk junction in Figs. 3(c) and 3(e) [41].

The above arguments can be exactly proven by both analytic and numerical solutions of Eq. (5) [11]. For the boundless $0-\pi$ disk junction in Fig. 3(c), the wave function of the first Majorana ZM takes the form $\psi_1(r, \theta) = [e^{-i\theta/2}u_\uparrow(r), e^{i\theta/2}u_\downarrow(r), e^{-i\theta/2}v_\downarrow(r), -e^{i\theta/2}v_\uparrow(r)]$ with the condition $u_\sigma(r) = -v_\sigma(r)$. $u_\sigma(r) = a_\sigma J_{\mp 1/2}(k_F r)e^{r/\xi_1}$ for $r < R_0$, and $u_\sigma(r) = b_\sigma J_{\mp 1/2}(k_F r)e^{-r/\xi_2}$ for $r > R_0$. $J_{\mp 1/2}(k_F r)$ are Bessel functions with $-1/2$ and $+1/2$ for spin up and down, respectively. a_σ and b_σ are coefficients determined by the continuity and normalization of the wave function. The Fermi wave vector $k_F = \mu/v_F$. The decay length $\xi_{1/2} = v_F/\Delta_{1/2}$. The wave function of the second Majorana ZM can be obtained by $\psi_2(r, \theta) = \mathcal{T}\psi_1(r, \theta)$. Note that the minigap to protect Majorana ZMs is proportional to v_F/R_0 , which ensures that only a pair of Majorana ZMs survive for small R_0 [11]. The STS-measured differential conductance $dI/dV \propto \sum_\sigma r[|u_\sigma(r)|^2\delta(\omega - eV) + |v_\sigma(r)|^2\delta(\omega + eV)]$. The case for Majorana ZMs is plotted in Fig. 4(b), from which the spatial profile of dI/dV is consistent with observations in monolayer Fe(Te,Se)/SrTiO₃ [7] but has a subtle difference near $r = 0$ in comparison to the measurements in bulk Fe(Te,Se) and LiFeAs [6,8]. We argue that this tiny difference is from effects of the IFI, such as the mixture of electronic states, the inelastic electron tunneling process, or finite quasiparticle scattering, etc. In Fig. 4(c), we consider modulation from finite quasiparticle scattering, and the resulting spectrum is quite similar to cases in bulk Fe(Te,Se) and LiFeAs [11]. For a finite $0-\pi$ disk junction, numerical results are also consistent with analytic solutions [11].

The aforementioned theory can be utilized to understand multiple features and common properties of ZMs in iron-based superconductors. We summarize the bound-state spectrum as the function $J(\mathbf{r} = 0, z_0)$ in Fig. 4(a). There exists a pair of near-zero-energy YSR states from the IFI when $J(\mathbf{r} = 0, z_0)$ is close to J_c . The electronlike and holelike components of a pair of near-zero-energy YSR states have opposite spin polarizations. Thus the whole of them shows no spin-resolved feature. When $J(\mathbf{r} = 0, z_0)$ is larger than J_c , a pair of near-zero-energy YSR states steeply split, and the robust Majorana ZMs emerge and are located at the

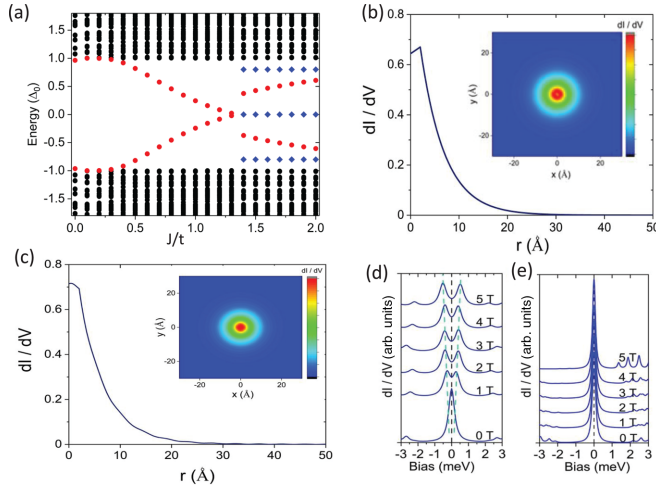


FIG. 4. (a) The overall energy spectrum from both YSR states (red) of IFI scattering and the Majorana ZMs (blue at zero energy) at the boundary separating the sign-change regimes as a function of $J(r=0, z)$. The former is the same as Fig. 2(a), and the latter is from the numerical solution of Eq. (4) defined in the finite disk configuration. (b) The simulated dI/dV profile for the Majorana zero mode from the analytic solutions of Eq. (4) defined in the boundless disk configuration. (c) The simulated dI/dV profile for the Majorana ZMs found by taking into account the quasiparticle scattering. The insets in (b) and (c) are the simulated dI/dV two-dimensional spatial profiles. (d) and (e) The external magnetic field effect for the YSR states and the Majorana ZMs, respectively.

boundary separated by two sign-change regimes. Note that the boundary is very close to the IFI. Thus the contradictions from different STM and STS experiments are rooted in the selected IFIs with different exchange couplings $J(\mathbf{r}=0, z)$, which coincides with the fact that ZMs can only be observed on partial IFIs [6–8]. The fragility of the near-zero-energy YSR state and the robustness of Majorana ZMs against an external magnetic field can also be understood. Consider the Zeeman energy m_z of an external magnetic field; for a pair of near-zero-energy YSR states, opposite spin polarization indicates that they have to split according to $m_z\sigma_z$, as shown in Fig. 4(d). For Majorana ZMs, the Hamiltonian $H_s(\mathbf{k} \rightarrow -i\nabla)$ defined in the $0-\pi$ disk junction possesses a hidden mirror symmetry $\mathcal{M}_{I=0} = i\sigma_y\tau_y\hat{O}(r)$. $\hat{O}(r)$ is a spatial inverse operator along the radial direction with inverse center at R_0 [11]. The degeneracy of a pair of Majorana ZMs is protected by this hidden mirror symmetry against the σ_z and σ_x Zeeman field. However, the in-plane Zeeman term $m_y\sigma_y$ can split the degeneracy of Majorana ZMs [42]. This behavior can be testified by future experimental measurements. Turning to the band structure, the Zeeman term m_z can be added into H_s in Eq. (4) to open a gap in the Dirac bands. Then, the solution forms of Majorana ZMs are not changed but have a modulated $k'_F = \sqrt{\mu^2 - m_z^2}/v_F$ [11]. Thus the Majorana ZMs are robust under the condition $m_z < \mu$, as shown in Fig. 4(e). Note that H_s plus $m_z\sigma_z$ is also one copy of the decoupled Hamiltonian describing the case in monolayer Fe(Te,Se)/SrTiO₃ [7],

in which Dirac bands are from the bulk. Some experiments have observed that Majorana ZMs disappear at a temperature below T_c [6–8]. This behavior can also be understood from the self-consistent calculation results in Fig. 2(d). The sign change $\Delta(r=0)$ decays to zero at about $T_q \sim 0.6T_c$. We argue that this is the primary reason for the temperature effect in spite of the possible quasiparticle poisoning [23,43]. It is worth noting that a magnetic impurity induced robust energy mode has also been observed in PbTaSe₂ [44], which also has topological bands and is superconducting. Within our theory, the observations in PbTaSe₂ can be well understood.

Finally, the reliability of the theory can be enhanced by estimating some relevant parameters. The first one is $J_c \sim 1.3t$ with t measuring the energy scale of the surface Dirac state, i.e., $t \sim v_F k_F$. According to experiments [23,45], $v_F \sim 250$ meV \AA^{-1} , and $k_F \sim 0.02$ \AA^{-1} . Then, $J_c \sim 7$ meV. This is also the reason why a single IFI with quite small exchange coupling can induce the QPT and relevant Majorana modes. The IFI can have a magnetic moment $m \sim 5 \mu_B$, which induces a magnetic dipole field $B(r) = \mu_0 m / 4\pi r^3$ [46,47]. The induced magnetic flux can be calculated by setting the lower limit of the integral cutoff to be the Wigner-Seitz radius of the square lattice. If one quantized magnetic vortex emerges, it requires that the magnetic moment increases to $10^4 \mu_B$, which is only possible for a magnetic cluster in the nanoscale.

In conclusion, we provide an alternative understanding to resolve the debate about whether STM- and STS-observed ZMs induced by IFIs on some iron-based superconductors are Majorana ZMs or not. We find that a QPT can be triggered by the exchange coupling between the IFI and the substrate. Then, the local superconducting order parameter of the surface superconducting state changes sign around the impurity, and we prove that a robust Kramers degenerate pair of Majorana ZMs can be induced and trapped around the IFI. Our theory can explain a series of confusing features observed in experiments. More meaningfully, our theory can be extended to other material categories, which host both topological bands and superconductivity.

The authors thank J. P. Hu, Z. Fang, C. Fang, X. X. Wu, S. B. Zhang, S. S. Qin, F. W. Zheng, H. F. Du, L. Shan, Z. Y. Wang, S. C. Yan, and X. Y. Hou for helpful discussions. This work was financially supported by the National Key R&D Program of China (Grants No. 2022YFA1403200 and No. 2017YFA0303201), the National Natural Science Foundation of China (Grants No. 92265104, No. 12022413, No. 11674331, and No. 11625415), the ‘‘Strategic Priority Research Program (B)’’ of the Chinese Academy of Sciences, Grant No. XDB33030100, the ‘‘100 Talents Project’’ of the Chinese Academy of Sciences, the Collaborative Innovation Program of Hefei Science Center, CAS (Grant No. 2020HSC-CIP002), the CASHIPS Director’s Fund (BJPY2019B03), the Science Challenge Project under Grant No. TZ2016001, and the Major Basic Program of the Natural Science Foundation of Shandong Province (Grant No. ZR2021ZD01). A portion of this work was supported by the High Magnetic Field Laboratory of Anhui Province, China.

- [1] L. Yu, Bound state in superconductors with paramagnetic impurities, *Acta Phys. Sin.* **21**, 75 (1965).
- [2] H. Shiba, Classical spins in superconductors, *Prog. Theor. Phys.* **40**, 435 (1968).
- [3] A. I. Rusinov, On the theory of gapless superconductivity in alloys containing paramagnetic impurities, *Sov. Phys. JETP* **29**, 1101 (1969).
- [4] J. Kondo, Resistance minimum in dilute magnetic alloys, *Prog. Theor. Phys.* **32**, 37 (1964).
- [5] A. V. Balatsky, I. Vekhter, and J.-X. Zhu, Impurity-induced states in conventional and unconventional superconductors, *Rev. Mod. Phys.* **78**, 373 (2006).
- [6] J.-X. Yin, Z. Wu, J.-H. Wang, Z.-Y. Ye, J. Gong, X.-Y. Hou, L. Shan, A. Li, X.-J. Liang, X.-X. Wu, J. Li, C.-S. Ting, Z.-Q. Wang, J.-P. Hu, P.-H. Hor, H. Ding, and S. H. Pan, Observation of a robust zero-energy bound state in iron-based superconductor Fe(Te,Se), *Nat. Phys.* **11**, 543 (2015).
- [7] C. Liu, C. Chen, X. Liu, Z. Wang, Y. Liu, S. Ye, Z. Wang, J. Hu, and J. Wang, Zero-energy bound states in the high-temperature superconductors at the two-dimensional limit, *Sci. Adv.* **6**, eaax7547 (2020).
- [8] P. Fan, F. Yang, G. Qian, H. Chen, Y.-Y. Zhang, G. Li, Z. Huang, Y. Xing, L. Kong, W. Liu, K. Jiang, C. Shen, S. Du, J. Schneeloch, R. Zhong, G. Gu, Z. Wang, H. Ding, and H.-J. Gao, Observation of magnetic adatom-induced Majorana vortex and its hybridization with field-induced Majorana vortex in an iron-based superconductor, *Nat. Commun.* **12**, 1348 (2021).
- [9] D. Wang, J. Wiebe, R. Zhong, G. Gu, and R. Wiesendanger, Spin-Polarized Yu-Shiba-Rusinov States in an Iron-Based Superconductor, *Phys. Rev. Lett.* **126**, 076802 (2021).
- [10] D. Chatzopoulos, D. Cho, K. M. Bastiaans, G. O. Steffensen, D. Bouwmeester, A. Akbari, G. Gu, J. Paaske, B. M. Andersen, and M. P. Allan, Spatially dispersing Yu-Shiba-Rusinov states in the unconventional superconductor $\text{FeTe}_{0.55}\text{Se}_{0.45}$, *Nat. Commun.* **12**, 298 (2021).
- [11] See Supplemental Material at <http://link.aps.org/supplemental/10.1103/PhysRevB.106.L180504> for details about the density functional theory (DFT) calculations, the self-consistent solutions of the BdG equations in the lattice model, the proof of the equivalence between the vortex case and the impurity case, and the solutions for the Majorana zero modes (see also Refs. [8,12–23] therein).
- [12] G. Kresse and J. Furthmüller, Efficient iterative schemes for *ab initio* total-energy calculations using a plane-wave basis set, *Phys. Rev. B* **54**, 11169 (1996).
- [13] G. Kresse and D. Joubert, From ultrasoft pseudopotentials to the projector augmented-wave method, *Phys. Rev. B* **59**, 1758 (1999).
- [14] P. E. Blöchl, Projector augmented-wave method, *Phys. Rev. B* **50**, 17953 (1994).
- [15] J. P. Perdew, K. Burke, and M. Ernzerhof, Generalized Gradient Approximation Made Simple, *Phys. Rev. Lett.* **77**, 3865 (1996).
- [16] A. I. Buzdin, Proximity effects in superconductor-ferromagnet heterostructures, *Rev. Mod. Phys.* **77**, 935 (2005).
- [17] J.-X. Zhu, W. Kim, C. S. Ting, and J. P. Carbotte, Quasiparticle States around a Nonmagnetic Impurity in a *d*-Density-Wave State of High- T_c Cuprates, *Phys. Rev. Lett.* **87**, 197001 (2001).
- [18] S. Raghu, X.-L. Qi, C.-X. Liu, D. J. Scalapino, and S.-C. Zhang, Minimal two-band model of the superconducting iron oxynictides, *Phys. Rev. B* **77**, 220503(R) (2008).
- [19] T. Kawakami and X. Hu, Evolution of Density of States and a Spin-Resolved Checkerboard-Type Pattern Associated with the Majorana Bound State, *Phys. Rev. Lett.* **115**, 177001 (2015).
- [20] H.-H. Sun, K.-W. Zhang, L.-H. Hu, C. Li, G.-Y. Wang, H.-Y. Ma, Z.-A. Xu, C.-L. Gao, D.-D. Guan, Y.-Y. Li, C. Liu, D. Qian, Y. Zhou, L. Fu, S.-C. Li, F.-C. Zhang, and J.-F. Jia, Majorana Zero Mode Detected with Spin Selective Andreev Reflection in the Vortex of a Topological Superconductor, *Phys. Rev. Lett.* **116**, 257003 (2016).
- [21] J. J. Sakurai, *Advanced Quantum Mechanics* (Addison-Wesley, New York, 1967).
- [22] L. Mao and C. Zhang, Robustness of Majorana modes and minigaps in a spin-orbit-coupled semiconductor-superconductor heterostructure, *Phys. Rev. B* **82**, 174506 (2010).
- [23] D. Wang, L. Kong, P. Fan, H. Chen, S. Zhu, W. Liu, L. Cao, Y. Sun, S. Du, J. Schneeloch, R. Zhong, G. Gu, L. Fu, H. Ding, and H.-J. Gao, Evidence for Majorana bound states in an iron-based superconductor, *Science* **362**, 333 (2018).
- [24] V. Thampy, J. Kang, J. A. Rodriguez-Rivera, W. Bao, A. T. Savici, J. Hu, T. J. Liu, B. Qian, D. Fobes, Z. Q. Mao, C. B. Fu, W. C. Chen, Q. Ye, R. W. Erwin, T. R. Gentile, Z. Tesanovic, and C. Broholm, Friedel-Like Oscillations from Interstitial Iron in Superconducting $\text{Fe}_{1+y}\text{Te}_{0.62}\text{Se}_{0.38}$, *Phys. Rev. Lett.* **108**, 107002 (2012).
- [25] N. Hao and J. Hu, Topological Phases in the Single-Layer FeSe, *Phys. Rev. X* **4**, 031053 (2014).
- [26] Z. Wang, P. Zhang, G. Xu, L. K. Zeng, H. Miao, X. Xu, T. Qian, H. Weng, P. Richard, A. V. Fedorov, H. Ding, X. Dai, and Z. Fang, Topological nature of the $\text{FeSe}_{0.5}\text{Te}_{0.5}$ superconductor, *Phys. Rev. B* **92**, 115119 (2015).
- [27] X. Wu, S. Qin, Y. Liang, H. Fan, and J. Hu, Topological characters in $\text{Fe}(\text{Te}_{1-x}\text{Se}_x)$ thin films, *Phys. Rev. B* **93**, 115129 (2016).
- [28] G. Xu, B. Lian, P. Tang, X.-L. Qi, and S.-C. Zhang, Topological Superconductivity on the Surface of Fe-Based Superconductors, *Phys. Rev. Lett.* **117**, 047001 (2016).
- [29] N. Hao and J. Hu, Topological quantum states of matter in iron-based superconductors: from concept to material realization, *Natl. Sci. Rev.* **6**, 213 (2019).
- [30] K. Jiang, X. Dai, and Z. Wang, Quantum Anomalous Vortex and Majorana Zero Mode in Iron-Based Superconductor Fe(Te,Se), *Phys. Rev. X* **9**, 011033 (2019).
- [31] X. Wu, S. B. Chung, C. Liu, and E.-A. Kim, Topological orders competing for the Dirac surface state in FeSeTe surfaces, *Phys. Rev. Res.* **3**, 013066 (2021).
- [32] Z. Zhou and J. Klinovaja, Zero-energy Andreev bound states in iron-based superconductor Fe(Te,Se), [arXiv:2109.08200](https://arxiv.org/abs/2109.08200).
- [33] M. E. Flatté and J. M. Byers, Local Electronic Structure of a Single Magnetic Impurity in a Superconductor, *Phys. Rev. Lett.* **78**, 3761 (1997).
- [34] R. Kümmel, Electronic structure of superconductors with dilute magnetic impurities, *Phys. Rev. B* **6**, 2617 (1972).
- [35] A. Yazdani, B. A. Jones, C. P. Lutz, M. F. Crommie, and D. M. Eigler, Probing the local effects of magnetic impurities on superconductivity, *Science* **275**, 1767 (1997).
- [36] M. I. Salkola, A. V. Balatsky, and J. R. Schrieffer, Spectral properties of quasiparticle excitations induced by magnetic moments in superconductors, *Phys. Rev. B* **55**, 12648 (1997).

- [37] T. Meng, J. Klinovaja, S. Hoffman, P. Simon, and D. Loss, Superconducting gap renormalization around two magnetic impurities: From Shiba to Andreev bound states, *Phys. Rev. B* **92**, 064503 (2015).
- [38] L. Fu and C. L. Kane, Superconducting Proximity Effect and Majorana Fermions at the Surface of a Topological Insulator, *Phys. Rev. Lett.* **100**, 096407 (2008).
- [39] R. Song, P. Zhang, and N. Hao, Phase-Manipulation-Induced Majorana Mode and Braiding Realization in Iron-Based Superconductor Fe(Te,Se), *Phys. Rev. Lett.* **128**, 016402 (2022).
- [40] W.-Y. Shan, J. Lu, H.-Z. Lu, and S.-Q. Shen, Vacancy-induced bound states in topological insulators, *Phys. Rev. B* **84**, 035307 (2011).
- [41] X.-L. Qi, T. L. Hughes, S. Raghu, and S.-C. Zhang, Time-Reversal-Invariant Topological Superconductors and Superfluids in Two and Three Dimensions, *Phys. Rev. Lett.* **102**, 187001 (2009).
- [42] F. Zhang, C. L. Kane, and E. J. Mele, Time-Reversal-Invariant Topological Superconductivity and Majorana Kramers Pairs, *Phys. Rev. Lett.* **111**, 056402 (2013).
- [43] J. R. Colbert and P. A. Lee, Proposal to measure the quasiparticle poisoning time of Majorana bound states, *Phys. Rev. B* **89**, 140505(R) (2014).
- [44] S. S. Zhang, J.-X. Yin, G. Dai, L. Zhao, T.-R. Chang, N. Shumiya, K. Jiang, H. Zheng, G. Bian, D. Multer, M. Litskevich, G. Chang, I. Belopolski, T. A. Cochran, X. Wu, D. Wu, J. Luo, G. Chen, H. Lin, F.-C. Chou *et al.*, Field-free platform for Majorana-like zero mode in superconductors with a topological surface state, *Phys. Rev. B* **101**, 100507(R) (2020).
- [45] P. Zhang, K. Yaji, T. Hashimoto, Y. Ota, T. Kondo, K. Okazaki, Z. Wang, J. Wen, G. D. Gu, H. Ding, and S. Shin, Observation of topological superconductivity on the surface of an iron-based superconductor, *Science* **360**, 182 (2018).
- [46] T. Choi, W. Paul, S. Rolf-Pissarczyk, A. J. Macdonald, F. D. Natterer, K. Yang, P. Willke, C. P. Lutz, and A. J. Heinrich, Atomic-scale sensing of the magnetic dipolar field from single atoms, *Nat. Nanotechnol.* **12**, 420 (2017).
- [47] T. Choi, C. P. Lutz, and A. J. Heinrich, Studies of magnetic dipolar interaction between individual atoms using ESR-STM, *Curr. Appl. Phys.* **17**, 1513 (2017).